# Strongly emissive individual DNA-encapsulated Ag nanoclusters as single-molecule fluorophores

**Tom Vosch, Yasuko Antoku, Jung-Cheng Hsiang, Chris I. Richards, Jose I. Gonzalez, and Robert M. Dickson***

School of Chemistry and Biochemistry and Petit Institute for Bioengineering and Bioscience, Georgia Institute of Technology, Atlanta, GA 30332-0400

Edited by Robert J. Silbey, Massachusetts Institute of Technology, Cambridge, MA, and approved April 2, 2007 (received for review December 4, 2006)

**The water-soluble, near-IR-emitting DNA-encapsulated silver nanocluster presented herein exhibits extremely bright and photostable emission on the single-molecule and bulk levels. The photophysics have been elucidated by intensity-dependent correlation analysis and suggest a heavy atom effect of silver that rapidly depopulates an excited dark level before quenching by oxygen, thereby conferring great photostability, very high single-molecule emission rates, and essentially no blinking on experimentally relevant time scales (0.1 to >1,000 ms). Strong antibunching is observed from these biocompatible species, which emit >$10^9$ photons before photobleaching. The significant dark-state quantum yield even enables bunching from the emissive state to be observed as a dip in the autocorrelation curve with only a single detector as the dark state precludes emission from the emissive level. These species represent significant improvements over existing dyes, and the nonpower law blinking kinetics suggest that these very small species may be alternatives to much larger and strongly intermittent semiconductor quantum dots.**

correlation | photophysics | silver nanoclusters | single-molecule spectroscopy | fluorescence intermittency

While myriad dyes exist with varying photophysical properties (1, 2), organic dye-based single-molecule and even bulk *in vivo* imaging dynamics studies suffer from low probe brightness, poor photostability (3), and oxygen sensitivity (4). Advances in nanotechnology such as the use of quantum dots (5, 6) have ameliorated some of these issues but at the cost of toxicity (7), broad excitation (8, 9), power-law blinking (10–12), and large probe size (13, 14). While quantum dots are readily excited with low-intensity sources, their fluorescence exhibits intermittency on all time scales (10–12), thereby causing problems when used for tracking or imaging studies. Arising from Auger processes (15), these photophysical dynamics are apparent at all excitation intensities and appear without characteristic times. While functionalization, large size (≈10–20 nm in diameter), and cellular uptake are potential problems, the strong nonmolecular power-law fluorescence intermittency is a major drawback of these materials as single-molecule reporters (10–12). Recently, ≈35-nm-sized fluorescent nanodiamonds have also been reported as single-molecule emitters, but these also raise concerns about label size (16). Consequently, for both *in vitro* and *in vivo* single-molecule studies, fluorophores with high emission rates and excellent photostability must be identified that are completely devoid of blinking on all relevant time scales, while maintaining small overall sizes.

By combining the virtues of chemistry and nanotechnology, we have developed few-atom, molecular-scale noble metal nanoclusters as a class of emitters that simultaneously exhibit bright, highly polarizable discrete transitions, good photostability, and small size, all within biocompatible scaffolds (17–20). Recent observations that DNA encapsulates Ag nanoclusters to yield a range of absorption and emission features throughout the visible region (21) have enabled the detailed investigation of Ag nanocluster size and nanocluster interactions with cytosine bases in particular (18, 20). Here, we report a bright, near-IR-emitting Ag nanocluster created in ssDNA consisting of 12 cytosine bases that shows very high emission rates, excellent photostability, strong antibunching, and essentially no intensity fluctuations on experimentally relevant time scales.

## Results and Discussion

We have used the demonstrated affinity between silver and cytosine bases on ssDNA (18, 22–27) to create near-IR-emitting Ag nanoclusters with excellent single-molecule and bulk optical properties. While we have separately reported the visible emitters in bulk studies (18, 20), the preferentially created ≈700-nm emitter reported here offers strong emission in a less-obscured spectral window and shows excellent single-molecule emission. These species were created by combining a $6 \times 10^{-5}$ M solution of single-stranded $C_{12}$ DNA (Integrated DNA Technologies, Coralville, IA) with $3.6 \times 10^{-4}$ M $AgNO_3$ (99.9999%; Aldrich, St. Louis, MO), both in 18-MΩ water, and reducing the Ag ions with one equivalent of $NaBH_4$ (98%; Sigma, St. Louis, MO). Upon reducing the $C_{12}$ DNA and $Ag^+$ mixture, small DNA-stabilized silver clusters are formed as schematized in Fig. 1*A*, without further growth into large nanoparticles. Upon adding $NaBH_4$ to the mixture of $C_{12}$ ssDNA and silver nitrate, two emissive species are formed that emit in the red and near-IR regions resulting from different $Ag_n$ cluster sizes. While multiple species can be created, dissolution in PBS preferentially creates an Ag nanocluster species that has an excitation maximum of ≈650 nm and emission maximum of ≈700 nm (Fig. 1*B*). This species has a fluorescence quantum yield of 17% and exhibits a 2.6-ns lifetime and a molar extinction coefficient of $3.2 \times 10^5$ $M^{-1}{\cdot}cm^{-1}$, as determined by fluorescence correlation spectroscopy (FCS). Gel electrophoresis combined with mass spectrometry analysis indicates that this species is either the Ag dimer or trimer, as both emitters are present even after purification [supporting information (SI) Fig. 4]. Additionally, although the observed stability in the presence of NaCl (21) and preferential formation in short DNA strands relative to all other emitters (unpublished work) (21) suggests that this is the highly stable (28) Ag dimer, reports of 620- and 700-nm emission from the Ag trimer in rare gas matrices (29) support the IR emitter being the trimer. Further studies will be necessary to better separate these two emitters.

Under identical imaging conditions, our near-IR-emitting nanoclusters appear at least twice as bright as Cy5.29 (Fig. 1 *C* and *D*). As the fluorescence quantum yields (0.17 for the IR-emitting $C_{12}$–$Ag_n$, 0.3 for Cy5.29) and the extinction coeffi-

Author contributions: R.M.D. designed research; T.V., Y.A., J.-C.H., C.I.R., and J.I.G. performed research; T.V., Y.A., J.-C.H., C.I.R., J.I.G., and R.M.D. analyzed data; and T.V. and R.M.D. wrote the paper.

The authors declare no conflict of interest.

This article is a PNAS Direct Submission.

Abbreviations: FCS, fluorescence correlation spectroscopy; ISC, intersystem crossing; CW, continuous wave; PAID, photon arrival-time interval distribution.

*To whom correspondence should be addressed. E-mail: dickson@chemistry.gatech.edu.

This article contains supporting information online at www.pnas.org/cgi/content/full/0610677104/DC1.

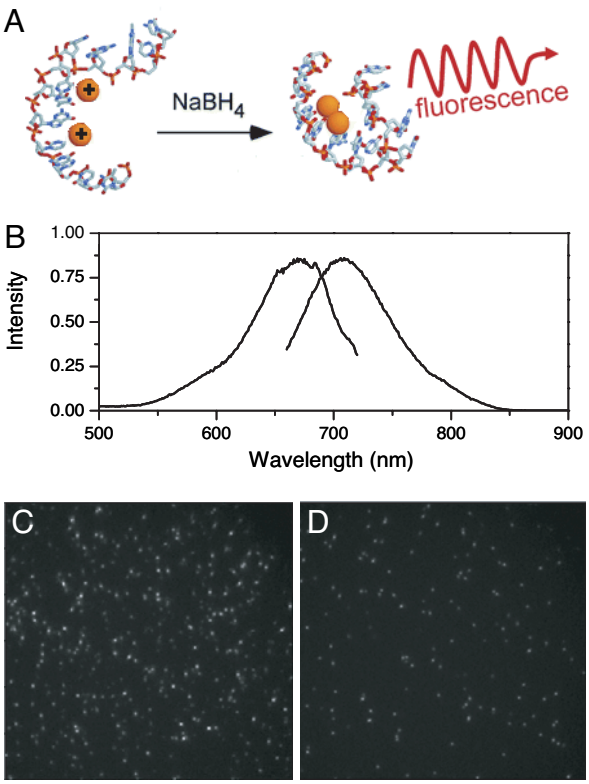


**Fig. 1.** Near-IR-emitting Ag nanoclusters. (*A*) Schematic of the IR-emitting $C_{12}$–$Ag_n$ formation. After complexation of $C_{12}$ DNA with silver cations, the mixture is reduced with $NaBH_4$ and the near-IR-emitting Ag nanocluster is studied. (*B*) Normalized excitation and emission spectra of the studied species. (*C*) Image of single IR-emitting $C_{12}$–$Ag_n$ molecules in a poly(vinyl alcohol) (PVA) film. (*D*) Image of single Cy5.29 molecules in a PVA film. The image dimensions are 40 × 40 $\mu$m, and imaging conditions of *C* and *D* are identical (Hg-lamp excitation through a 640- to 660-nm bandpass filter at ≈5W/cm$^2$ and detected with identical settings on an Andor iXon CCD).

cients ($3.2 \times 10^5$ $M^{-1}\cdot cm^{-1}$ for the IR-emitting $C_{12}$–$Ag_n$, $2.5 \times 10^5$ $M^{-1}\cdot cm^{-1}$ for Cy5.29) roughly offset, the increased brightness of IR-emitting $C_{12}$–$Ag_n$ under weak excitation (≈5 W/cm$^2$ incident intensity) likely arises from significant differences in blinking dynamics. Although the photophysics and blinking of Cy5 fluorophores are well known (30, 31) and can be minimized (32) or used to one's advantage (31, 33), like all organic dyes, $O_2$ sensitivity, moderate photobleaching quantum yields ($\approx 10^{-6}$), and intensity-dependent blinking time scales that obscure true dynamics of the system under study all seriously limit application in single-molecule studies. Excited at 647 nm under ambient conditions, single-nanocluster emission rates increase sublinearly with excitation intensity (Fig. 2*A*), presumably because of intersystem crossing (ISC) dynamics. Unlike organic fluorophores, Ag nanoclusters show essentially no blinking on experimentally relevant time scales (0.1 to >1,000 ms), while exhibiting excellent photostability. At lower excitation intensities (≈1 kW/cm$^2$), 10 kcps is readily detected for many minutes to hours. Fig. 2*B* shows an example of a typical single molecule excited with 633-nm continuous wave (CW) excitation (1.5 kW/cm$^2$), which had an average detected fluorescence intensity of ≈25,000 counts per s for 1,250 s after which the molecule bleached or transitioned into a long-lived off state. Although devoid of intensity fluctuations on normal experimental/binning time scales, autocorrelation traces of both immobilized molecules (Fig. 2*C* and Table 1) and those free in solution as measured by FCS (Table 1) show fast intensity fluctuations on the tens of

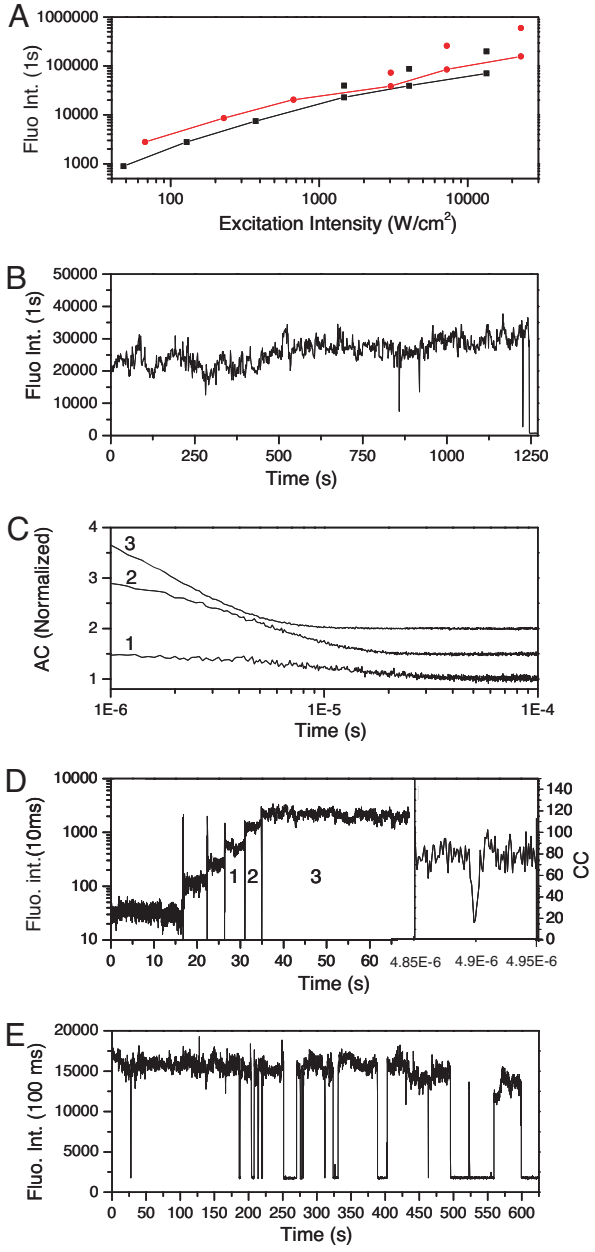


**Fig. 2.** High emission rates and intensity-dependent photphysics of $C_{12}$-$Ag_n$. (*A*) Fluorescence intensity versus excitation intensity curves for 647-nm (red) and 633-nm excitation (black). The connected scatter points correspond to the average fluorescence intensity, while the unconnected scatter points correspond to the burst fluorescence intensity level in the on period. The latter are only presented for the three highest fluorescence intensities. (*B*) Fluorescence intensity trajectory of a single IR-emitting $C_{12}$-$Ag_n$ molecule excited at 633-nm CW excitation and an excitation intensity of 1,500 W/cm$^2$. (*C*) Autocorrelation traces of the three brightest intensity levels from *D*. The numbers from 1 to 3 correspond to the levels indicated in *D*. The autocorrelation curves were constructed by using bin times of 100 ns, and curves 2 and 3 are vertically offset by 0.5 and 1.0, respectively for clarity. (*D*) Fluorescence intensity trajectory of a single molecule excited with CW 647 nm as incident intensity is changed from 67 to 230, 670, 3,000, 7,200, and 23,000 W/cm$^2$. Vertical lines demarcate intensity changes. The right section shows the zero-delay portion [one channel is artificially delayed by ≈4.9 $\mu$s with a DG-535 delay generator (Stanford Research, Sunnyvale, CA) to avoid detection dead times] of the photon arrival cross-correlation (CC) of a molecule excited with 23,000 W/cm$^2$ using a bin time of 1 ns. This region shows the antibunching feature of the fluorescence from the excited state. (*E*) Fluorescence intensity trajectory of a single IR-emitting $C_{12}$–$Ag_n$ molecule excited at 647 nm using an excitation intensity of 23,000 W/cm$^2$.

**Table 1. Experimental and extracted photophysical parameters from the IR-emitting $C_{12}$– $Ag_n$ emitters**

| $\lambda_{exc}$, nm | Excitation intensity, W/cm$^2$ | $\tau_c$, $\mu$s | Average intensity, counts/s | Burst intensity, counts/s | $\tau_{off}$, $\mu$s | $\tau_{on}$, $\mu$s | $k_{ISC}$, $10^6$ s$^{-1}$ | $\phi_{ISC}$, $10^{-3}$ |
|---|---|---|---|---|---|---|---|---|
| 647 | 6.72E+01 | | 2,600 | | | | | |
| 647 | 2.28E+02 | | 7,700 | | | | | |
| 647 | 6.72E+02 | | 17,500 | | | | | |
| 647 | 1.13E+03 | 11.7 | 31,400 | 57,300 | 20$\sigma$:8 | 29$\sigma$:16 | 3.2$\sigma$:2.8 | 8.4$\sigma$:7.5 |
| 647 | 3.04E+03 | 9.4 | 33,000 | 73,300 | 18$\sigma$:5 | 20$\sigma$:11 | 3.3$\sigma$:1.7 | 8.7$\sigma$:4.4 |
| 647 | 7.22E+03 | 3.5 | 67,200 | 261,300 | 10$\sigma$:3.5 | 5.3$\sigma$:2.6 | 4.0$\sigma$:1.9 | 9.7$\sigma$:5.3 |
| 647 | 2.28E+04 | 1.9 | 128,100 | 596,200 | 5.5$\sigma$:1.9 | 2.9$\sigma$:1.7 | 3.8$\sigma$:2.1 | 9.3$\sigma$:5.6 |
| 647 | 2.81E+03 | 4.9* | | | | | | |
| 633 | 4.81E+01 | | 1,000 | | | | | |
| 633 | 1.28E+02 | | 2,800 | | | | | |
| 633 | 3.73E+02 | | 7,900 | | | | | |
| 633 | 1.47E+03 | 20.9 | 20,400 | 34,600 | 29$\sigma$:13 | 73$\sigma$:23 | 2.9$\sigma$:3 | 7.9$\sigma$:7.9 |
| 633 | 4.03E+03 | 14.8 | 36,000 | 78,000 | 22$\sigma$:7 | 47$\sigma$:10 | 2.7$\sigma$:2.4 | 7.7$\sigma$:6.8 |
| 633 | 1.34E+04 | 8.9 | 60,500 | 173,700 | 14$\sigma$:5 | 26$\sigma$:4 | 3.7$\sigma$:4.2 | 11$\sigma$:12 |

*Measured by FCS.

microseconds scale resulting from excited-state transitions into a dark state. Assuming a three-level system with fluctuations arising from ISC, the correlation decay time is a combination of on and off times (Eqs. **1** and **2**), corresponding to the dark-state formation quantum yield and dark-state lifetime, respectively (34, 35). Further suggesting ISC dynamics, the correlation time decreases with increasing excitation intensity (Fig. 2 *C* and *D*). As the correlation decay is given by Eqs. **1** and **2**, this often-observed correlation time shortening with excitation intensity typically arises from a shortened "on" time (i.e., increased rate of ISC), while not changing $\tau_{off}$. Expected to lengthen the off time, oxygen exclusion ($10^{-6}$ torr) did not alter the correlation decay at any intensity level (data not shown). This fast decay component therefore likely arises from a heavy atom effect of silver that enhances the rates both into and out of a spin forbidden state, such that the dark-state lifetime is faster than quenching by oxygen, yielding the observed oxygen insensitivity, fast dark-state decay, and extreme photostability. As molecules detected by FCS sample vastly different intensities as they traverse different regions of the excitation volume, comparisons of intensity-dependent photophysical parameters with those of immobilized species are somewhat inappropriate. The similar correlation decays to those of immobilized molecules (Table 1), however, indicates that aqueous and immobilized molecule photophysics are very similar, even with the increased range of motion available in solution. Consequently, long time photophysics and parameters are extracted only from immobilized species, with the understanding that these appear similar to those free in solution.

With increased excitation intensity, emission rates continue to increase to levels normally unattainable with current organic fluorophores and without bleaching. These higher excitation intensities yield upwards of 200,000 cps (detected; Fig. 2 *D* and *E*), but at the expense of blinking with long on and off times that are easily discriminated by a single threshold (Fig. 2*E*). The number of events is currently too low to determine consensus time scales. Currently thought to be a multiphoton process based on higher power-pulsed data, more extensive intensity-dependent long-time blinking dynamics need to be examined in future studies. With CW excitation, the long off times are quite rare and only appear at the very highest excitation intensities, further suggesting multiphoton origins. Although emission rates and photostabilities are more reminiscent of much larger semiconductor quantum dots than of organic fluorophores, the single exponential blinking dynamics only on very fast time scales demonstrates that these are molecular species that should improve on the problematic power-law blinking of quantum dots (10–12) for single-molecule tracking studies.

Modeling observed photophysics by a three-level system at all intensity levels one can directly extract $\tau_{on}$ and $\tau_{off}$, and, consequently, the ISC rate constant, $k_{isc}$, from fitting the correlation function [$C(t)$, with correlation time $\tau_c$] coupled with independently measured relevant experimental and molecular photophysical parameters (Eqs. **1–4**) (34).

$$C(t) = A + Be^{-t/\tau_c} \quad [1]$$

$$1/\tau_c = 1/\tau_{on} + 1/\tau_{off} \quad [2]$$

$$\tau_{on}/\tau_{off} = A/B \quad [3]$$

$$k_{isc} = \phi_{fl}\phi_{eff}/(\tau_{fl}\tau_{on}I_{on}). \quad [4]$$

In these equations, $\Phi_{fl}$ is the fluorescence quantum yield (0.17), $\Phi_{eff}$ is the experimental detection efficiency (0.05), $\tau_{fl}$ is the fluorescence lifetime, $\tau_{on}$ and $\tau_{off}$ are the on and off times, and $I_{on}$ is the intensity/bin while in the on state.

Extracted intensity-dependent molecular photophysical parameters were similar for both 647-nm and 633-nm CW excitation (Table 1). Interestingly, the shortened correlation decay at high excitation intensities results from not only the expected decreased on time (i.e., more cycles through the emissive state per second), but also a decreased off time. Both excitation wavelengths at high enough incident intensity shorten the dark-state lifetime, thereby enabling more photons per second to be obtained from individual molecules. Intrinsic dark-state lifetimes are $\approx$30 $\mu$s, but decrease to $<$10 $\mu$s for the highest excitation intensities, significantly increasing the duty cycle (rate) of emission. In other words, instead of having to wait for some long time for the dark state to decay, dark-state absorption and back ISC significantly shortens the off time, yielding many more excitation cycles per second to be achieved.

The value of $\tau_{on}$ naturally decreases with increasing excitation intensity, yielding an average $k_{isc}$ of $3.3 \times 10^7$ s$^{-1}$. This relatively high ISC rate indicates a dark-state quantum yield of $\approx$0.9% and causes the on time for the highest intensity level to be comparable to or shorter than the off time, thereby demonstrating the importance of shortening the dark-state lifetime with increasing intensity to yield bright emission. Consequently, the actual fluorescence intensity while in the on state is significantly higher than the value one obtains from binning the data in long intervals (e.g., 0.1 or 1 s). This instantaneous fluorescence intensity is represented in Table 1 as "burst" intensity, and the average

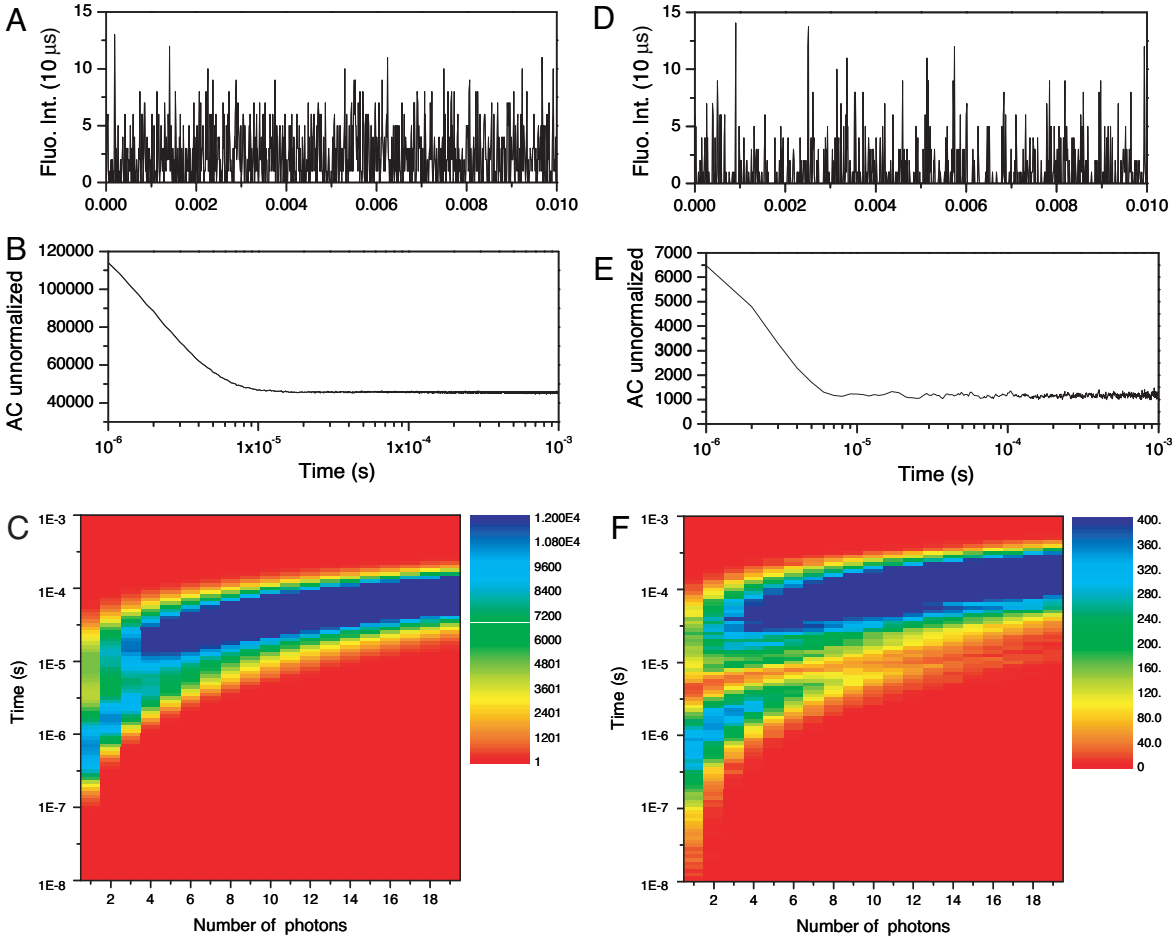


**Fig. 3.** Short-lived dark state directly observed through protein bunching. (*A*) Fluorescence intensity trajectory of a single IR-emitting $C_{12}$–$Ag_n$ molecule in 10-$\mu$s time bins. (*B*) Autocorrelation of the data depicted in A. (*C*) PAID histogram of the data depicted in *A*. (*D*) Simulation of fluorescence intensity trajectory of a single molecule, using the same photophysical parameters as obtained from fitted data of the molecule depicted in *A*, binned in 10 $\mu$s. (*E*) Autocorrelation of the data depicted in *D*. (*F*) PAID histogram of the data depicted in *D*. Triplet modulation of the singlet emission can only be seen upon spreading correlations along an axis giving the numbers of photons between each correlated pair, which uniquely enables bunching to be observed with a single detector at much longer times. Experimental and simulated emission traces show nearly identical features.

intensity is reported as the fluorescence intensity in 0.1-s intervals. Fig. 2*A* shows the evolution of the fluorescence intensity versus excitation intensity on a log/log scale. In Fig. 2*A* the red connected curve corresponds to 647-nm excitation, and the black connected curve corresponds to 633-nm excitation. This average emission becomes sublinear at high excitation intensities and tends toward saturation. The black and red scatter points that are not connected to the curves in Fig. 2*A* show the burst intensities, which increasingly deviate from the average intensities as excitation intensity increases, further indicating that the dark state limits the overall emission rate. The detected fluorescence from 633-nm excitation is roughly half that of the value excited at 647 nm at the same excitation intensity, reflecting the relative molar extinctions at 633 and 647 nm (Fig. 1*B*).

To demonstrate the remarkable photostability, Fig. 2*E* shows a typical single nanocluster excited at 647 nm (23 kW/cm$^2$), that during this 650-s trace enabled $>10^8$ photons to be collected before it transitioned to a long-lived off state. Assuming 5% detection efficiency, this trajectory corresponds to $>2 \times 10^9$ emitted photons and $>10^{10}$ excitation cycles. If one uses excitation intensities near 1 kW/cm$^2$, intensity traces are readily recorded for several hours with virtually no long-term blinking. At high excitation intensities, we observe occasional transitions into usually recoverable long-lived dark states, but because of the length of these off periods, it is difficult to say whether or not we observe photobleaching. At low excitation intensities, typically, the only intensity fluctuations on time scales $>100$ $\mu$s result from mechanical instability and refocusing.

Although blinking is generally accepted evidence of single quantum system observation, the apparent lack of intensity fluctuations at low excitation intensity and achievable extremely high emission rates seemingly contradict our assertion that these are single molecules. Consequently, using two detectors in a Hanbury Brown-Twiss setup (17, 36) and introducing a delay between the two avalanche photodiode channels of 4.9 $\mu$s, we time-stamped the arrival times of all photons detected in both channels and performed a cross-correlation, which shows excellent antibunched emission from the IR-emitting $C_{12}$–$Ag_n$ species at all observed emission rates (Fig. 2*D Right*). CW antibunching requires extreme photostability and high emission rates, further indicating the promise of these materials and providing the only conclusive proof of single-molecule emission.

Amazingly, the high ISC quantum yield and intensity-dependent dark-state lifetime also offer the unique opportunity to observe bunched emission from the emissive level due to the dark-state dynamics. Like emission from individual ions (37), single-molecule emission is bunched and antibunched on multiple characteristic time scales (35). Individual fluorescence photons are, of course,

antibunched at times corresponding to the inverse radiative rate, resulting in the near-zero probability of two photons being detected simultaneously within the single molecule's emissive lifetime (e.g., Fig. 2*D*). Photons also appear bunched together, however, for on times that are characteristic of the inverse ISC rate, leading to dark or off levels. The duration of the off states are then characteristic of the dark-state lifetime (34). Consequently, if the dark-state yield is sufficiently large and the on and off times sufficiently short, bunching of fluorescence photons due to ISC dynamics should be observable at longer times, such that a fluorescence photon should not be observable while the molecule is in its dark-state level. In other words, the dark state should modulate the emission by preventing photons from being emitted while in this level. Such bunching would appear at much longer times and should be observable with a single detector, but the bunching feature would need to be observed on a relatively high background of photons from the emissive state. Recently, photon arrival-time interval distributions (PAIDs) (38) have been used to stretch correlations in two dimensions with the correlation time between photon pairs being along one axis and the number of photons between a given pair plotted along the other. Collapsing all data to the former axis gives the standard correlation function, whereas collapsing all data to the latter gives photon count histograms (39). For our single nanocluster emission and simulated molecules with identical photophysical parameters, taking time differences between all photon pairs and noting the number of photons detected between each pair directly enables construction of these PAID histograms (Fig. 3). While the autocorrelations (Fig. 3*B*) show no dip at $\approx 8$ $\mu$s, the PAID histogram clearly shows a dip in this region that corresponds to the intensity anticorrelation resulting from dark-state shelving. The autocorrelation of simulated data gives very similar autocorrelation curves and PAID histograms as the actual data, with the observable dip at $\approx 8$ $\mu$s when the photons are spread out in two dimensions as with the experimental data. These anticorrelations cannot be readily observed in the standard autocorrelation curves because of the low contrast relative to emitted photons. Time-tagged photon arrival times were simulated as a three-level system with photophysical parameters as obtained from the actual experimental data. Single molecules are modeled as Poisson emitters of a given emission intensity but modified by finite emissive-level and dark-state lifetimes, such that no emission can occur within the exponentially distributed lifetimes of these states. A time base of 1 ns was used, creating a digital trace mimicking the experimental data such that the average number of photons per bin is well below 1 for every intensity level. In this way we simulated time-tagged photon arrival data streams and analyzed them with the same software used for analyzing the experimental data. Therefore, the unique photophysics of these stable oligonucleotide-encapsulated fluorophores enable direct single-molecule evidence by observing the bunching feature at times exceeding detection dead times. The fact that on levels are only detected with $\approx 5\%$ (detection efficiency), but off levels are detected with near perfect fidelity, makes PAID analysis ideal for verifying single-molecule biomolecular observation.

## Conclusions

ssDNA-encapsulated Ag nanoclusters yield highly stable and bright fluorescence in the near IR. The very high emission rates without blinking on experimentally relevant time scales (0.1 to >1,000 ms) and the excellent photostability enable shorter and longer time dynamics of individual molecules to be followed than possible with any other fluorophores. The unique photophysics not only confer outstanding optical properties in aqueous solution, but also enable a single-molecule-specific bunching feature to be observed at long times due to ISC modulation of fluorescence. These few-atom Ag species offer great potential in pushing *in vitro*, and possibly *in vivo*, single-molecule studies to much faster and also much longer time scales than currently possible.

## Methods

Steady-state absorption and fluorescence spectra of the $C_{12}$–$Ag_n$ complex in deionized water were recorded on a UV-2401 PC spectrophotometer (Shimadzu, Kyoto, Japan) and a PTI fluorometer (Photon Technology International, Lawrenceville, NJ), respectively. FCS was performed with a ×60, 1.2 N.A. water immersion objective to focus laser excitation light into solution. Fluorescence collected by this objective as molecules diffused through the diffraction-limited volume was focused on a 100-$\mu$m multimode fiber and routed to one or two avalanche photodiodes. Serial dilutions from initial solutions for which absorbance at 650 nm was measured enabled determination of molar absorptivities through FCS-based counting of emitters in the calibrated detection focal volume (40). Time-stamped arrival times enabled correlation functions to be calculated for times less than the diffusive transit time through the detection volume, similar to that described below for immobilized molecules. Immobilized single-molecule experiments were performed by diluting 1 $\mu$l of a buffered (borate buffer, pH 9) DNA-encapsulated silver cluster solution in 999 $\mu$l of saturated aqueous poly(vinyl alcohol) (5 mg/ml, 98% hydrolyzed, 16,000 MW; Acros Organics, Geel, Belgium) solution and spun-coat on a cleaned glass coverslip at 1,500 rpm for 1 min. (P-6000 Spin Coater model P6204; Special Coating Systems, Indianapolis, IN). Coverslips were cleaned by sequential sonication in acetone, 1 M NaOH, and milliQ water (18 MΩ), each for 15 min. The coverslips were then rinsed with milliQ water, dried with compressed $N_2$, and put in a UV ozone photo reactor (PR-100; Ultra Violet Products, San Gabriel, CA) for 2 h. For molecule visualization and positioning, a CCD camera (Ixon; Andor, South Windsor, CT) and a scanning stage (MS2000; Applied Scientific Instruments, Eugene, OR) were used. Fluorescence data from the single $C_{12}$–$Ag_n$ molecules was collected through a ×100, 1.4 N.A. oil immersion objective on an IX70 inverted microscope (Olympus, Melville, NY) with appropriate emission filters and routed to one or two avalanche photodiodes (SPAQ; PerkinElmer, Wellesley, MA) with appropriate delays and arrival times recorded with a SPC630 card (Becker-Hickl, Berlin, Germay). A CW 647-nm laser (air-cooled mixed gas laser; Melles Griot, Irvine, CA) and a CW 633-nm laser (HeNe laser; Melles Griot) were used for excitation. To get CW antibunching data, the macro and micro times of each photon detection event were properly combined to create an absolute time. For this we expanded on the approach by Weston *et al.* (41) to use the macro timer as a poor stopwatch to determine the number of sync cycles that have passed between two photon detection events and replaced this value with the more precise value of a multiple of the measured sync period. From this value we subtract the micro time to get the absolute photon detection time.

T.V. was supported by a Fonds Voor Wetenschappelijk Onderzoek postdoctoral fellowship. R.M.D. was supported by National Science Foundation Grant BES-0323453 and National Institutes of Health Grants R01GM68732 and P20GM072021.

1. Schmidt T, Kubitscheck U, Rohler D, Nienhaus U (2002) *Single Mol* 3:327.
2. Vosch T, Cotlet M, Hofkens J, Van der Biest K, Lor M, Weston K, Tinnefeld P, Sauer M, Latterini L, Mullen K, *et al.* (2003) *J Phys Chem A* 107:6920–6931.
3. Eggeling C, Widengren J, Rigler R, Seidel CAM (1998) *Anal Chem* 70:2651–2659.
4. Lill Y, Hecht B (2004) *Appl Phys Lett* 84:1165–1167.
5. Empedocles SA, Norris DJ, Bawendi MG (1996) *Phys Rev Lett* 77:3873–3876.
6. Aichele T, Zwiller V, Benson O (2004) *New J Phys* 6:90–102.
7. Derfus AM, Chan WCW, Bhatia SN (2004) *Nano Lett* 4:11–18.
8. Dabbousi BO, RodriguezViejo J, Mikulec FV, Heine JR, Mattoussi H, Ober R, Jensen KF, Bawendi MG (1997) *J Phys Chem B* 101:9463–9475.

9. Norris DJ, Bawendi MG (1995) *J Chem Phys* 103:5260–5268.
10. Verberk R, Van Oijen AM, Orrit M (2002) *Phys Rev B* 66:233202.
11. Zhang K, Chang HY, Fu AH, Alivisatos AP, Yang H (2006) *Nano Lett* 6:843–847.
12. Kuno M, Fromm DP, Hamann HF, Gallagher A, Nesbitt DJ (2000) *J Chem Phys* 112:3117–3120.
13. Bruchez M, Moronne M, Gin P, Weiss S, Alivisatos AP (1998) *Science* 281:2013–2016.
14. Chan WCW, Nie SM (1998) *Science* 281:2016–2018.
15. Klimov VI, Mikhailovsky AA, McBranch DW, Leatherdale CA, Bawendi MG (2000) *Science* 287:1011–1013.
16. Fu CC, Lee HY, Chen K, Lim TS, Wu HY, Lin PK, Wei PK, Tsao PH, Chang HC, Fann W (2007) *Proc Nat Acad Sci USA* 104:727–732.
17. Peyser-Capadona L, Zheng J, Gonzalez JI, Lee TH, Patel SA, Dickson RM (2005) *Phys Rev Lett* 94:058301.
18. Petty JT, Zheng J, Hud NV, Dickson RM (2004) *J Am Chem Soc* 126:5207–5212.
19. Zheng J, Dickson RM (2002) *J Am Chem Soc* 124:13982–13983.
20. Ritchie CM, Johnsen KR, Kiser JR, Antoku Y, Dickson RM, Petty JT (2007) *J Phys Chem C* 111:175–181.
21. Antoku Y (2007) PhD thesis (Georgia Institute of Technology, Atlanta).
22. Braun E, Eichen Y, Sivan U, Ben-Yoseph G (1998) *Nature* 391:775–778.
23. Niemeyer C (2001) *Angew Chem Int Ed* 40:4128–4158.
24. Richter J, Seidel R, Kirsch R, Mertig M, Pompe W, Plaschke J, Schackert HK (2000) *Adv Mater* 12:507–510.
25. Richter J, Mertig M, Pompe W, Monch I, Schackert HK (2001) *Appl Phys Lett* 78:536–538.
26. Mertig M, Ciacchi LC, Seidel R, Pompe W, De Vita A (2002) *Nano Lett* 2:841–844.
27. Monson CF, Woolley AT (2003) *Nano Lett* 3:359–363.
28. Linnert T, Mulvaney P, Henglein A, Weller H (1990) *J Am Chem Soc* 112:4657–4664.
29. Schulze W, Rabin I, Ertl G (2004) *Chem Phys Chem* 5:403–407.
30. Huang ZX, Ji DM, Xia AD (2005) *Colloids Surf* 257/258:203–209.
31. Heilemann M, Margeat E, Kasper R, Sauer M, Tinnefeld P (2005) *J Am Chem Soc* 127:3801–3806.
32. Rasnik I, McKinney SA, Ha T (2006) *Nat Methods* 3:891–893.
33. Bates M, Blosser TR, Zhuang XW (2005) *Phys Rev Lett* 94:108101.
34. Yip WT, Hu DH, Yu J, Vanden Bout DA, Barbara PF (1998) *J Phys Chem A* 102:7564–7575.
35. Orrit M (2002) *Single Mol* 3:255–265.
36. Kumar P, Lee TH, Mehta A, Sumpter BG, Dickson RM, Barnes MD (2004) *J Am Chem Soc* 126:3376–3377.
37. Diedrich F, Walther H (1987) *Phys Rev Lett* 58:203–206.
38. Laurence TA, Kapanidis AN, Kong XX, Chemla DS, Weiss S (2004) *J Phys Chem B* 108:3051–3067.
39. Chen Y, Müller JD, So PTC, Gratton E (1999) *Biophys J* 77:553–567.
40. Enderlein J, Gregor I, Patra D, Dertinger T, Kaupp UB (2005) *Chem Phys Chem* 6:2324–2336.
41. Weston KD, Dyck M, Tinnefeld P, Müller C, Herten DP, Sauer M (2002) *Anal Chem* 74:5342–5349.